Dual Band Split Ring Monopole Antenna Structures for 5G and WLAN Applications

Shubhangi Verulkar, Alka Khade, Mahadu Trimukhe, and Rajiv K. Gupta[*]

Abstract—In this paper, dual-band split ring monopole antenna structures for 5G sub-6 GHz and WLAN applications are proposed. The antenna structures are designed from a rectangular annular ring monopole antenna. A compact dual rectangular split ring monopole antenna is designed to operate over dual bands. The two split rings are connected through a common arm. The structure is optimized to provide $S_{11} \leq -10$ dB over 3.3–3.6 GHz and 5.15–5.5 GHz for 5G and WLAN applications. In the second dual-band antenna, a slot is cut in one of the arms to form another closed rectangular ring to further reduce the dimensions of the antenna. This structure provides $S_{11} \leq -10$ dB over 3.3–3.6 and 5.5–5.9 GHz for 5G, WLAN and V2X applications. The two bands can be easily controlled as the dimensions of two rings determine the resonant frequencies of the two bands, and one of the arms of a ring is unresponsive to lower band and affects upper band only. Both antennas offer nearly omnidirectional radiation patterns in both bands. The two prototype antennas are fabricated on a $0.17\lambda_0 \times 0.19\lambda_0$ and $0.15\lambda_0 \times 0.19\lambda_0$ FR4 substrate, where λ_0 is the free-space wavelength corresponding to 3.3 GHz. The measured results agree with the simulated ones.

1. INTRODUCTION

The demand and growth of mobile communication systems have increased significantly in recent years. Wireless technology is continuously evolving and has led us to the fifth generation (5G) technology. The ever increasing hunger for enhanced performance, improved functionality, low development cost, and small size is the driving force for technology development. Seamless connectivity, high data rate, low latency, and reliable access are some of the features which have opened flood gates for 5G technologies and deployment of 5G networks. In portable wireless systems, antennas are designed which can provide better performance to enhance the functionality of the systems at lower development cost with reduced size. Multiband antennas not only reduce the size and cost but also enhance the functionality of the system. Therefore, the rapid growth of mobile communication systems has forced researchers to design novel multiband antennas.

Conventionally, multi-band monopole antennas are designed using multiple branches. Each branch provides a different current patch and resonates at a different frequency. The effective length and width of a branch determine the resonant frequency and bandwidth of a branch. To reduce the size of antenna, these branches are designed in different shapes like meander-line, C shape, G shape, L shape, U shape, etc. [1–3]. Stubs, slots, and slits are introduced in radiating element and ground plane to obtain the desired bandwidth [4–7]. A monopole antenna is designed using inverted G shape and meander-line branches to achieve tri-band operation [1]. Arc-shaped strips with dual inverted L-shaped parasitic stubs are used to design a multiband antenna in [2]. A U shaped, clip shaped, F shaped, and X shaped multi-branch multiband monopole antenna is reported in [3]. A multiband antenna using folded open

stub and L-shaped strips on asymmetric trapezoid ground plane is designed in [4]. Inverted L- and Pi-shape slots [5] and an inverted L-shape slot [6] are introduced in rectangular patch to design a multiband antenna on a defected ground structure. Multiple resonating stubs in a defected ground plane are used to design a multiband antenna in [7].

Multiband antennas are also designed using fractal techniques [8–10]. Branches are added in a binary tree fractal bionic structure to design a dual-band antenna [8], while circle and triangle fractals by cutting triangular slots in a circular monopole are used to design a multiband antenna [9]. Elliptical shape fractal geometry on a defected ground is designed to achieve multibands in [10]. Slots and slits in radiating patch and ground plane offer an opportunity for reconfigurable antennas. Reconfigurable multi-band antennas have been reported [11–13]. A nested capacitive slot multiband reconfigurable antenna is designed by incorporating PIN diodes in the slots [11]. A tri-band reconfigurable antenna is designed by using PIN diodes in a rectangular slot ring at the bottom of the antenna [12]. PIN diodes are used in slots of radiating and ground plane to achieve reconfigurability and enhance the device utility [13].

Multiband antennas using annular ring and meta-material inspired split-ring resonator (SRR) are designed in [14–22]. An elliptical-ring with a split-triangular patch [14] and two connected rings [15] are used in designing a flexible dual-band and a transparent tri-band antenna, respectively. A sleeve-shaped dipole combined with a rectangular ring cage shaped dipole [16], an elliptical ring shaped [17] and dual square ring shaped [18] dual-band antennas have been reported. Dual-band antennas using meta-material inspired dual rectangular split ring [19] and electric inductive capacitive coupled hexagonal ring [20] have been designed. Complementary SRR (CSRR) [21] and Non-Bianisotropic CSRR [22] are engraved in rectangular patch to achieve dual and tri-band characteristics. Slots, annular ring, SRR, and CSRR are employed to miniaturize the dimensions of antenna. However, all these structures have large dimensions as compared to the proposed antenna.

In this paper, two compact dual-band antenna structures are proposed. In the first structure, a compact dual rectangular split ring monopole antenna is designed to operate over 3.3–3.6 GHz and 5.15–5.5 GHz for 5G and WLAN applications. The two split rings are connected through a common arm. In the second dual-band antenna, a slot is cut in one of the arms to form a closed rectangular ring. The antenna operates over 3.3–3.6 GHz and 5.5–5.9 GHz. The two bands can be easily controlled as the dimensions of two rings determine the resonant frequencies of the two bands, and one of the arms of a split ring is unresponsive to lower band and affects upper band only. The two antennas are designed and fabricated on a low cost and easily available FR4 substrate. Both the antennas offer nearly omnidirectional radiation characteristics.

2. DESIGN THEORY AND ANTENNA GEOMETRY

In a rectangular ring monopole antenna (RRMPA), the slot acts as a capacitor, and as a result, the impedance becomes more capacitive. Therefore, RRMPA resonates at lower frequency than a rectangular monopole antenna (RMPA). A slot cut in one side of RRMPA gives rise to a split ring monopole antenna (SRMPA); it results in the increase in capacitance of the structure and decrease in the resonant frequency. The resonant frequency can be tuned as it depends on the dimensions of the slot. The addition of a vertical arm at the center of the SRMPA results in the formation of two rings, where one closed ring loads the other split ring. The resonant frequency increases due to decrease in the dimension of split ring. A slot in the closed ring results in a double split ring monopole antenna (DSRMPA) and a dual-band monopole antenna. The position of the vertical arm determines the dimensions of two rings and controls the lower and upper bands. The two bands can be tuned easily.

The geometry of the two proposed antennas (PA1 and PA2) is shown in Fig. 1. The optimum dimensions of various parameters of proposed antennas are listed in Table 1. The evolution of the proposed antenna is shown in Fig. 2. The proposed antenna is designed from a rectangular monopole antenna, 'Antenna 1'. An $11 \times 15\,\text{mm}^2$ rectangular monopole is designed on a 1.6 mm thick FR4 substrate. The dimension of substrate is $20 \times 20\,\text{mm}^2$, and permittivity and loss tangent of FR4 substrate are 4.4 and 0.02, respectively. The structures are simulated using IE3D simulator. The lowest frequency corresponding to VSWR = 2 or $S_{11} = -9.5\,\text{dB}$ is given by [23, 24]

$$f_L = 72/(L + W/2\pi + g) \times k \tag{1}$$
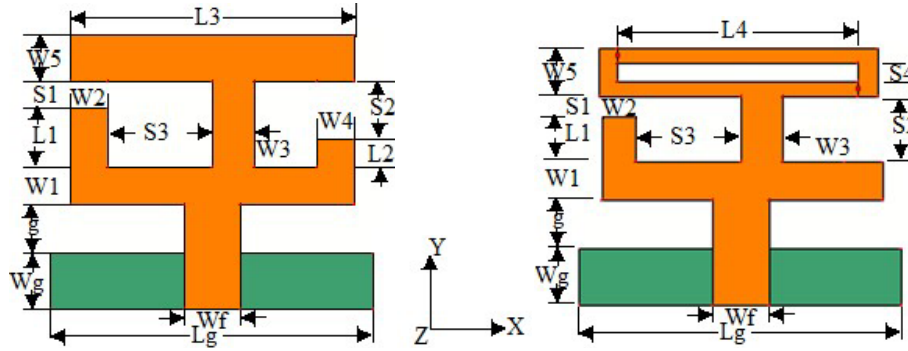
Figure 1. Geometry of proposed antenna structures.

Table 1. Optimized parameters of the proposed antennas (all dimensions in mm).

First Proposed Antenna PA1														
L_g	W_g	W_f	G	$W1$	$W2$	$W3$	$W4$	$W5$	$L1$	$L2$	$L3$	$S1$	$S2$	$S3$
17	3.0	3	2.5	2.0	2.0	2.2	2.0	2.5	3.1	1.5	15	1.4	3.0	5.5
Second Proposed Antenna PA2														
L_g	W_g	W_f	G	$W1$	$W2$	$W3$	$W5$	$L1$	$L3$	$L4$	$S1$	$S2$	$S3$	$S4$
17	3.0	3	2.5	2.0	2.0	2.2	2.5	2.4	14.7	12.7	1.1	3.5	5.5	1.0
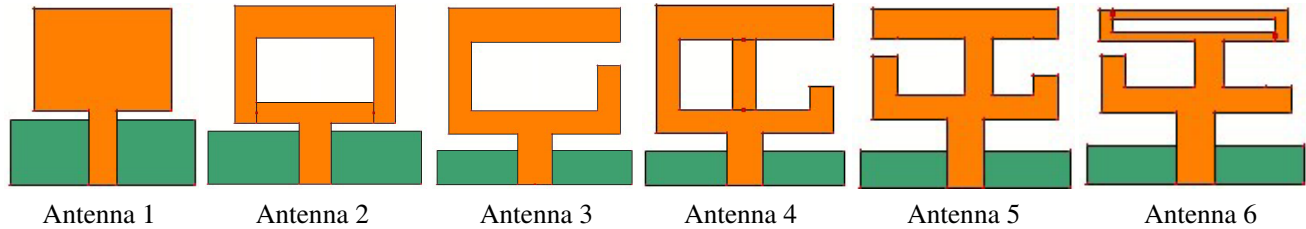
Figure 2. Evolution stages of the proposed antenna.

where L, W, and g are the length, width, and the gap between the radiating patch and ground plane, respectively, in millimeter, and f_L is in GHz. The value of $k = 1.15$ is considered for the FR-4 substrate [24]. The simulated f_L is 4.3 GHz while the calculated f_L is 4.34 GHz ($L = 11$ mm, $W = 15$ mm, and $g = 1.0$ mm). In rectangular monopole antenna (RMPA), 'Antenna 1', minimum S_{11} ($S_{11\,\mathrm{min}}$) occurs at 6.15 GHz, and it provides $S_{11} \leq -10$ dB over 4.38–8.0 GHz.

In a rectangular monopole antenna (RMPA), the resonant frequency depends on the physical dimensions of the antenna. The inductance of antenna is due to surface current on the conducting surface area of antenna while the capacitance can be attributed to substrate, radiating patch, ground plane, and the gap between radiating patch and ground plane.

When a slot is etched in RMPA to form a rectangular ring monopole antenna (RRMPA) 'Antenna 2', it increases the capacitive effect, and the impedance curve shifts downward as evident from Fig. 3. The increase in capacitance of the structure results in the decrease in f_L and frequency of $S_{11\,\mathrm{min}}$ as shown in Fig. 3. As the effective width of rectangular ring monopole antenna decreases, its impedance bandwidth also decreases. $S_{11\,\mathrm{min}}$ in RRMPA occurs at 5.0 GHz, and it provides $S_{11} \leq -10$ dB over 4.19–6.08 GHz. S_{11} and Impedance variation of RMPA and RRMPA are shown in Fig. 3. The impedance variation plot depicts a smaller loop for RRMPA than RMPA indicating that RRMPA has less impedance bandwidth than RMPA.
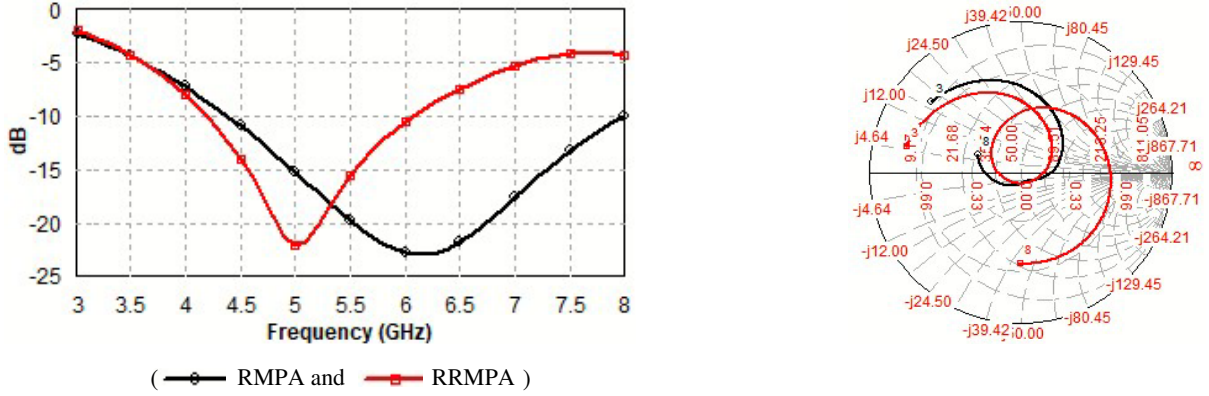
Figure 3. S_{11} and impedance variation.

Now a slot is cut in one side of the RRMPA to form a split ring monopole antenna (SRMA), 'Antenna 3'. The slot acts as a capacitor, and the impedance of the structure becomes capacitive. Due to the increase in the capacitance of the structure, the resonant frequency decreases. The capacitance decreases with the increase in slot length '$S2$', and as a result, the frequency of $S_{11\,min}$ increases with the increase in slot length. Impedance variation plot shifts upward with the increase in slot length. S_{11} and impedance variations for different slot lengths are shown in Fig. 4.
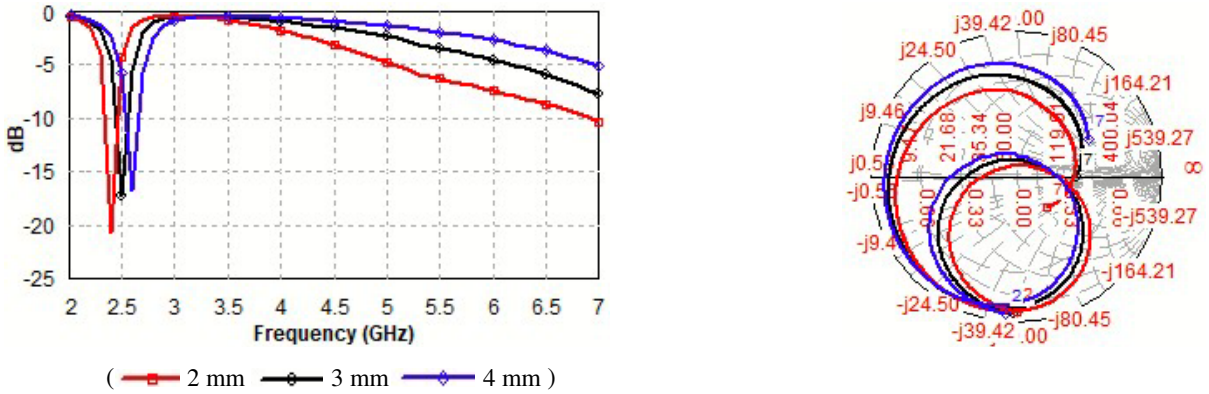
Figure 4. S_{11} and impedance variation for different $S2$.

In 'Antenna 4', a vertical arm is placed in the center of 'Antenna 3' to split it into two rings. A closed ring loads the split ring of Antenna 3; therefore, the resistance of the structure decreases, and the inductance increases. As a result, the impedance curve shifts left-upward as shown in Fig. 5. As the dimensions of the slotted ring decreases in 'Antenna 4', the resonant frequency of the structure increases. The addition of vertical arm also decreases the effective surface current in the slotted ring which results in the decrease in effective current path length and increase in resonant frequency. The slotted ring dimensions decrease, and therefore the frequency of $S_{11\,min}$ increases with the increase in $S3$ or when the vertical arm is shifted right, as shown in Fig. 5. The close ring electromagnetically couples with the split ring, and the position of vertical arm determines the coupling between the two rings. The coupling increases, and the loop area of impedance variation curve decreases with the increase in $S3$. Thus, the frequency of $S_{11\,min}$ of 'Antenna 4' depends on the position and dimensions of vertical arm and slot.

In 'Antenna 5', a second slot is etched in the other closed ring, to operate the structure over another band. A slot in closed ring results in a double split ring monopole antenna (DSRMPA) to operate over dual band. The parameters of this antenna are optimized. $S_{11} \leq -10\,\mathrm{dB}$ is obtained over 3.3–3.6 GHz

Figure 5. S_{11} and impedance variation for different $S3$.

and 5.15–5.51 GHz. The position of the vertical arm determines the dimensions of the two rings and controls the lower and upper bands. The two bands can be tuned easily. This proposed antenna 'PA1' is designed on a 15 mm × 17 mm substrate.

In 'Antenna 6', a slot is introduced in the center of the top arm of 'Antenna 5'. The current in the top rectangular ring has an inductive effect while the slot has a capacitive effect. The capacitive effect dominates at lower frequency band while inductive effect dominates at higher frequency band. The increase in capacitive effect over lower band results in the decrease in the resonant frequency of lower band, while the increase in inductive effect over upper band results in the decrease in resonant frequency of upper band. The dimensions of structure are decreased, and parameters of 'Antenna 6' are optimized. $S_{11} \leq -10$ dB is obtained over 3.3–3.6 GHz and 5.51–5.91 GHz. This proposed antenna 'PA2' has substrate dimensions of 14 mm × 17 mm. S_{11} and impedance variation of Antenna 5, 'PA1' and Antenna 6, 'PA2' are depicted in Fig. 6.

Figure 6. S_{11} and impedance variation of proposed antennas.

The lumped equivalent circuit models of evolution stages of the proposed antenna are depicted in Fig. 7. The feed line has a characteristic impedance Z_0, length l_f, and resistance R_f. It is common in all antennas but shown in equivalent circuit model of Antenna 1 only. The rectangular monopole antenna or 'Antenna 1' can be represented by a parallel combination of $R1$, $L1$ and $C1$ [21]. A slot is etched in RMPA to form RRMPA or 'Antenna 2'. A slot acts as a capacitor but change in metallic conducting area also affects the inductance and resistance. Therefore, 'Antenna 2' can be represented by a parallel combination of $R2$, $L2$, and $C2$. In 'Antenna 3', a slot is cut to form a split ring. A metallic conducting strip can be represented by an inductor, and a slot or a gap can be represented by a capacitor. The capacitance of the structure increases due to the slot in metallic ring, and therefore, its equivalent

Figure 7. Equivalent circuit model of evolution stages of proposed antenna.

circuit has an additional capacitor. A split ring is represented as a parallel combination of inductor and capacitor [21]. In 'Antenna 4', a vertical arm is placed, and thus a closed ring loads the split ring which increases the inductance. Therefore, 'Antenna 4' has an inductor $L4'$ in series with $L4$ which are in parallel combination with $R4$ and C4. 'Antenna 5' or the proposed antenna has two split rings which are connected through a vertical metallic arm. The two split rings are represented by a parallel combination of $L5$ and $C5$ and $L5'$ and $C5'$, while the common vertical metallic arm is represented by $L5''$. A slot in the top arm in 'Antenna 6' acts as a capacitor, while the metallic conducting ring acts as an inductor. Therefore, the equivalent circuit model of 'Antenna 6' has an additional capacitor $C6''$ and $L6''$ in series with $L6$ and $L6'$.

The resonant frequency and bandwidth of two bands depend on the number of parameters. In a monopole antenna ground plane length and width and the gap between radiating patch and ground plane affect the resonant frequency and bandwidth of antenna. In the proposed structures, resonant frequency and the bandwidth of two bands depend on the dimensions of slots $S1$, $S2$, $S3$ and widths $W1$, $W2$, $W3$, $W4$, $W5$. A parametric study is carried out to analyze the effect of different parameters on the first proposed structure. The effects of 'g' and slot $S4$ etched in the first proposed antenna are also analyzed.

The capacitance of split ring depends on slot dimensions. The resonant frequency increases as the capacitance decreases with the increase in slot dimension. The increase in dimensions of '$S1$' increases the frequencies of $S_{11\,min}$ of both the bands, whereas the increase in the dimensions of '$S2$' increases the frequency of $S_{11\,min}$ of upper band and has negligible effect on lower band. Thus '$S2$' can independently control the upper band. Similarly, the increase in the width '$W2$', lower arm of left split ring, decreases the inductance, decreases the dimensions of split ring, and increases the capacitance. The capacitive effect dominates over the inductive effect, which results in a slight decrease in frequencies of $S_{11\,min}$ of both the bands. The change in the width '$W4$', the lower arm of right split ring, has negligible effect on lower band, and it has little effect on upper band. S_{11} for different '$S1$' and '$S2$' are shown in Fig. 8, and S_{11} for different '$W2$' and '$W4$' are shown in Fig. 9. The slot dimensions affect the resonant frequency more than the width of the arm. The lower arm of right split ring does not affect the lower band as it is unresponsive to radiations at lower band which is explained subsequently with the help of surface current distribution.

The resonance frequency of a rectangular ring monopole antenna depends on the mean perimeter, slot dimensions, and width of the conducting arms of the ring. The capacitive effect is due to the slot in

(a) (—■— 0.9 mm　—○— 1.4 mm　—◇— 1.9 mm)　　　(b) (—■— 2.5 mm　—○— 3.0 mm　—◇— 3.5 mm)
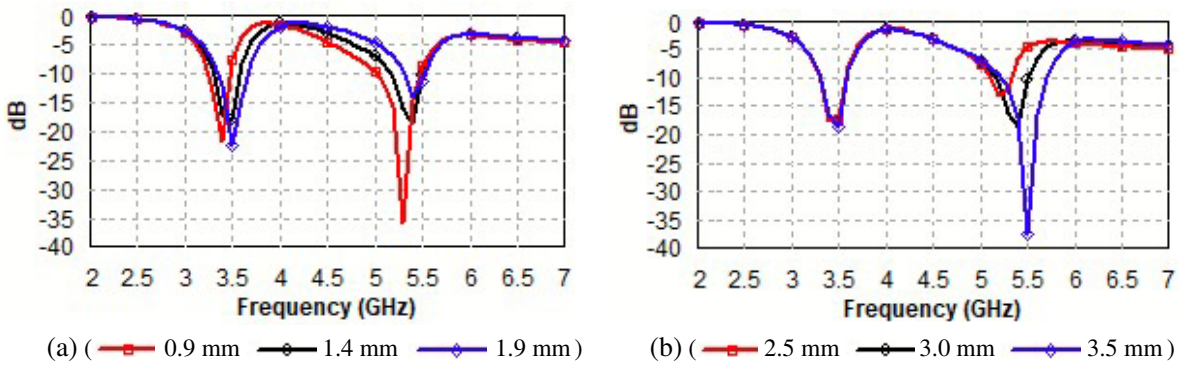
Figure 8. S_{11} and impedance variation for different (a) $S1$, (b) $S2$.

(a) (—■— 1.0 mm　—○— 2.0 mm　—◇— 3.0 mm)　　　(b) (—■— 1.0 mm　—○— 2.0 mm　—◇— 3.0 mm)
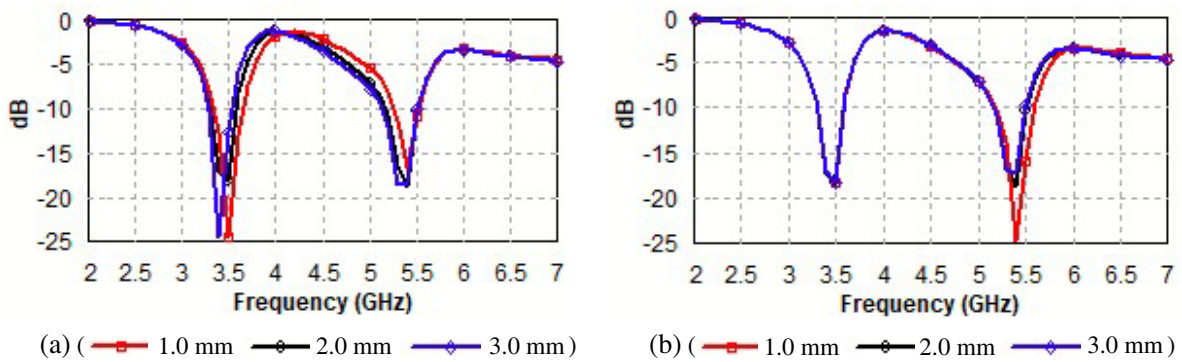
Figure 9. S_{11} and impedance variation for different (a) $W2$, (b) $W4$.

(a) (—■— 5.0 mm　—○— 5.5 mm　—◇— 6.0 mm)　　　(b) (—■— 1.7 mm　—○— 2.2 mm　—◇— 2.7 mm)
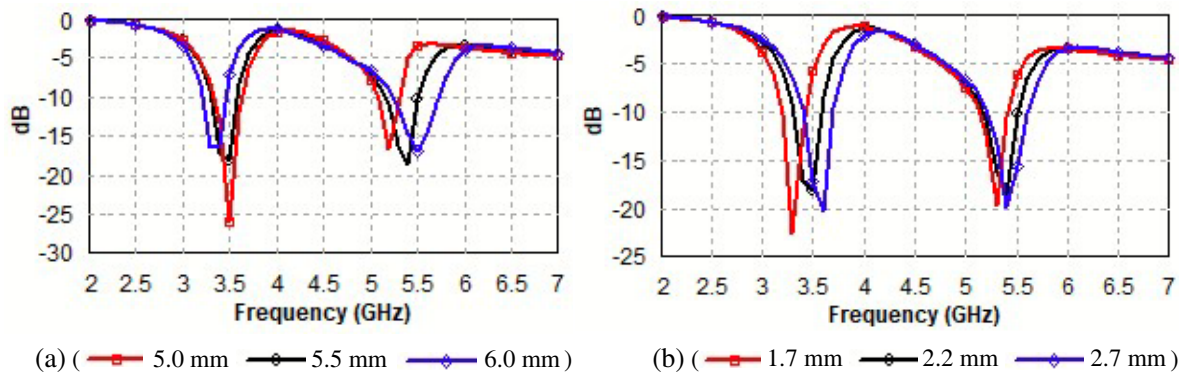
Figure 10. S_{11} for different (a) $S3$, (b) $W3$.

the rectangular ring, while the inductive effect in a rectangular ring is due to the current in conducting arms of rectangular ring.

As the mean perimeter of left split ring increases, that of right split ring decreases with the increase in '$S3$'. Therefore, the frequency of $S_{11\,\text{min}}$ of lower band decreases while that of upper band increases with the increase in '$S3$'. A small change in the perimeter of right split ring affects its frequency of $S_{11\,\text{min}}$ more as right split ring resonates at higher frequency. Therefore, with the increase in '$S3$', the increase in frequency of $S_{11\,\text{min}}$ of upper band is more than the decrease in frequency of $S_{11\,\text{min}}$ of lower band as shown in Fig. 10. The decrease in width '$W3$ of vertical arm increases the slot dimensions of both the split rings; therefore, it decreases the capacitance of split rings. However, the decrease in the width of conducting arm and increase in mean perimeter increase the inductance. The inductive effect
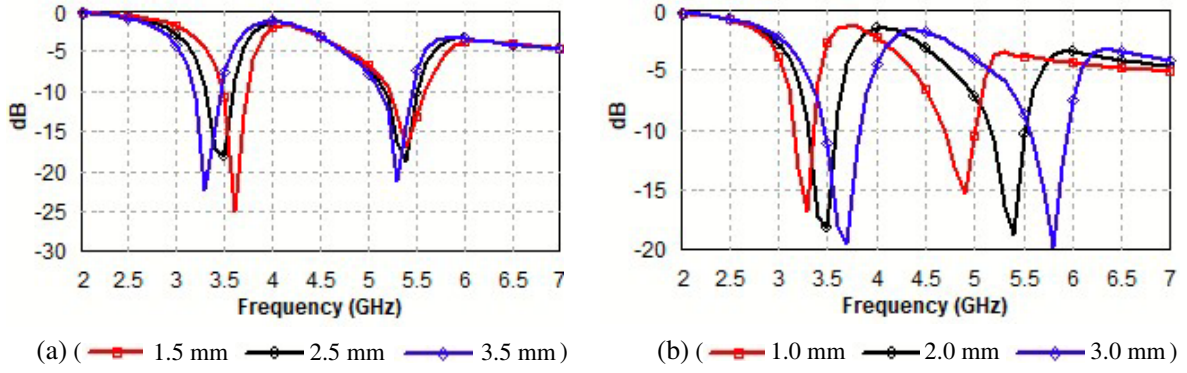
Figure 11. S_{11} for different (a) $W5$, (b) $W1$.
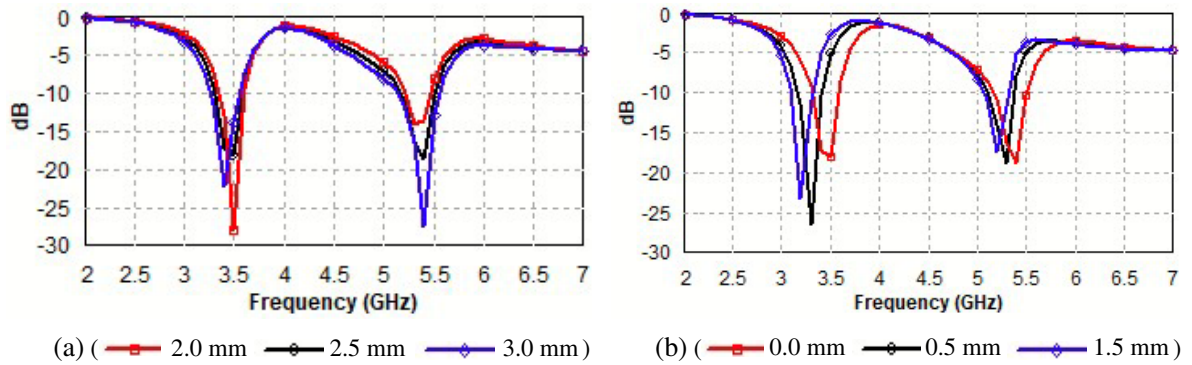
Figure 12. S_{11} for different (a) g, (b) $S4$.

dominates over capacitive effect. Therefore, the frequencies of $S_{11\,\text{min}}$ of both the bands decrease with the decrease in '$W3$' due to the increase in inductance of the structure as shown in Fig. 10.

The decrease in width '$W5$' of upper arm decreases the capacitance of split rings. The decrease in width of the arm also increases the inductance. The decrease in $W5$ also decreases the mean perimeter of two rings and thus decreases the inductance. As the surface current in the upper arm is less, the capacitive effect dominates over the inductive effect. As a result, the impedance of the structure becomes less capacitive, and the frequencies of $S_{11\,\text{min}}$ of both the bands increase with the decrease in '$W5$' as shown in Fig. 11. The decrease in width '$W1$ of the lower arm decreases the capacitance of split rings. The decrease in the width of conducting arm also results in the increase in the inductance. The decrease in $W1$ also increases $L1$, $L2$ and mean perimeter of two rings which also increase the inductance. The inductive effect dominates over capacitive effect as the surface current density is more in the lower arm than upper arm. The impedance of the structure becomes more inductive with the decrease in '$W1$', and therefore, the frequencies of $S_{11\,\text{min}}$ of both the bands decrease with the decrease in '$W5$' as shown in Fig. 11.

The gap between the ground plane and radiating patch acts as a matching network with the gap acting as a capacitor and the metallic strip acting as an inductor. Thus gap 'g' must be optimized for impedance matching. As 'g' increases, the resonant frequencies of two bands decrease slightly as shown in Fig. 12. A slot is etched in the center of the upper arm of the proposed antenna 'PA1'. The current in the rectangular ring has an inductive effect while the slot has a capacitive effect. The capacitive effect dominates at lower frequency band while inductive effect dominates at higher frequency band. The increase in capacitance of the structure over lower band results in decrease in resonant frequency of lower band, while the increase in inductance of the structure over upper band results in the decrease in resonant frequency of upper band. As the slot dimension '$S4$' increases, the frequency of $S_{11\,\text{min}}$ of both the bands decreases with the increase in $S4$ as shown in Fig. 12. Therefore, the dimensions of
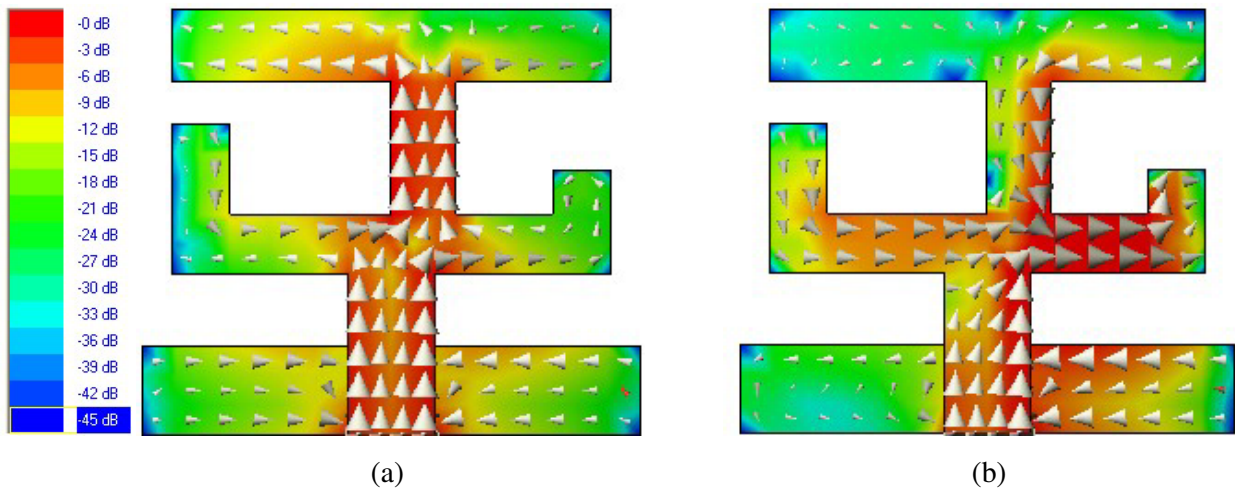
Figure 13. Scalar and vector surface current distribution of proposed antenna PA1, (a) 3.45 GHz, (b) 5.25 GHz.
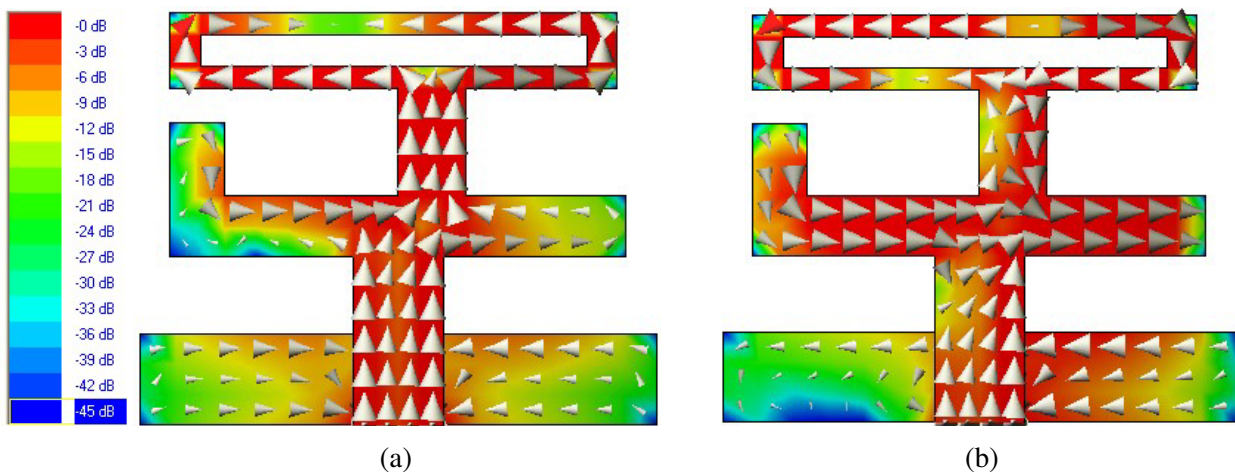
Figure 14. Scalar and vector surface current distribution of proposed antenna PA2, (a) 3.45 GHz, (b) 5.8 GHz.

structure are decreased, and parameters of the proposed antenna 'PA2' are optimized. $S_{11} \leq -10$ dB is obtained over 3.3–3.6 GHz and 5.51–5.91 GHz.

The dual-band characteristics of the proposed antenna PA1 and PA2 can be explained with the help of surface current distribution shown in Fig. 13 and Fig. 14, respectively. The surface current is mainly concentrated in the left ring at 3.45 GHz, while it is concentrated in the right split ring at 5.25 GHz in PA1 and 5.8 GHz in PA2. In both PA1 and PA2, at 3.45 GHz, vector surface current forms a loop in the lower arm of the right split ring; therefore, the lower arm of the right split ring becomes unresponsive and does not radiate. As a result, the dimensions of this arm do not affect the resonant frequency and bandwidth of the lower band and affect only upper band. Thus the upper band can be controlled independently by optimizing the dimensions of this arm. The surface current distribution of PA2 shows that there is considerable increase in surface current density in the upper arm when a slot is etched in the upper arm of PA1.

Top view-PA1   bottom view-PA1   Top view-PA2   bottom view-PA2
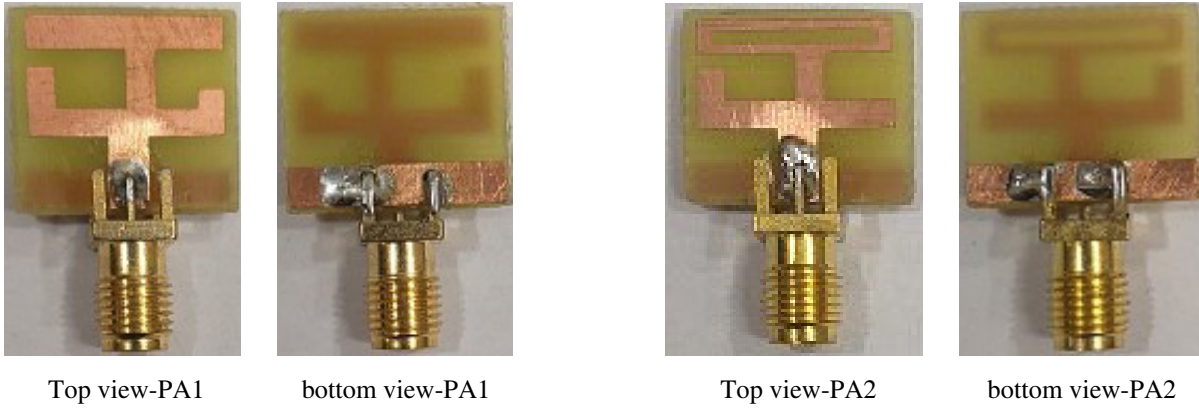
Figure 15. Fabricated prototype of proposed antenna structures PA1 and PA2.
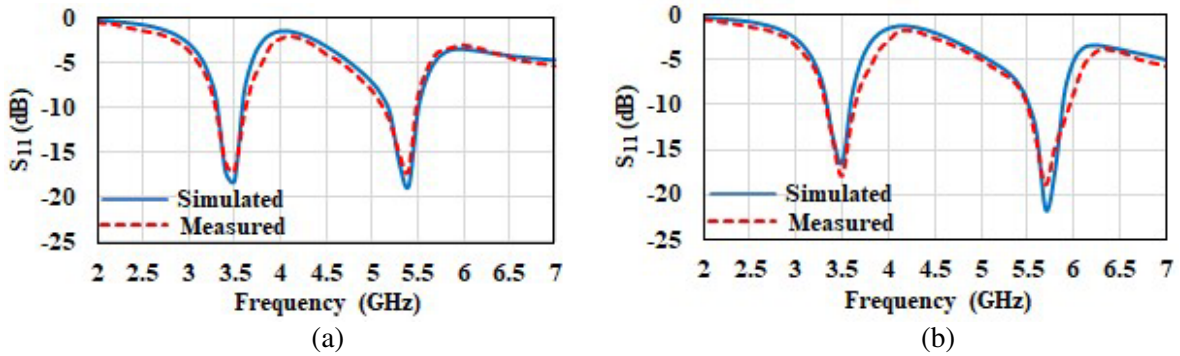
Figure 16. Measured and simulated S_{11} of proposed antenna structures, (a) PA1, (b) PA2.
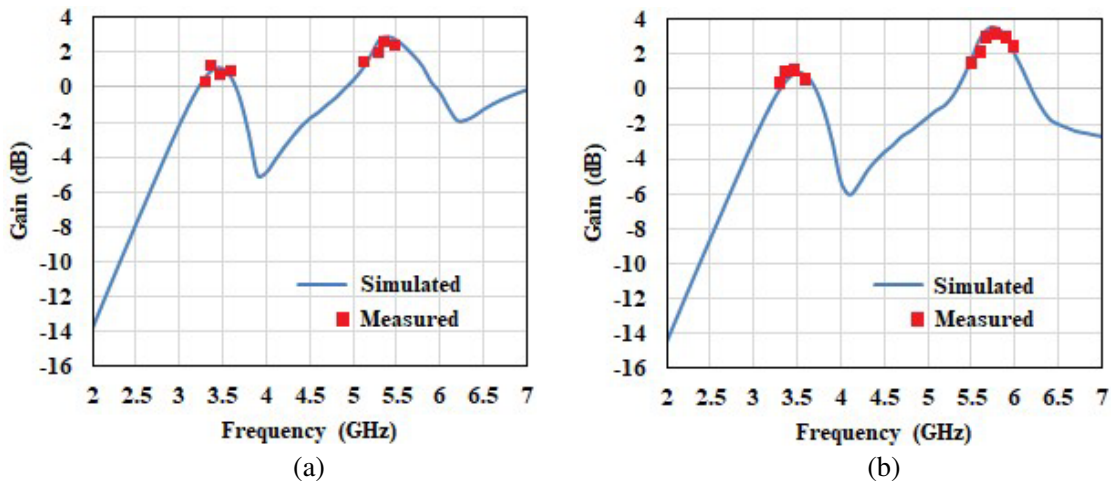
Figure 17. Measured and simulated gain of proposed antenna structures, (a) PA1, (b) PA2.

3. FABRICATION AND MEASURED RESULTS

The fabricated prototypes of proposed antenna structures PA1 and PA2 are shown in Fig. 15. The return loss (S_{11}) is measured using 9916A Agilent network analyzer, and gain and radiation patterns are measured using a standard wideband horn antenna in an anechoic chamber. Simulated and measured
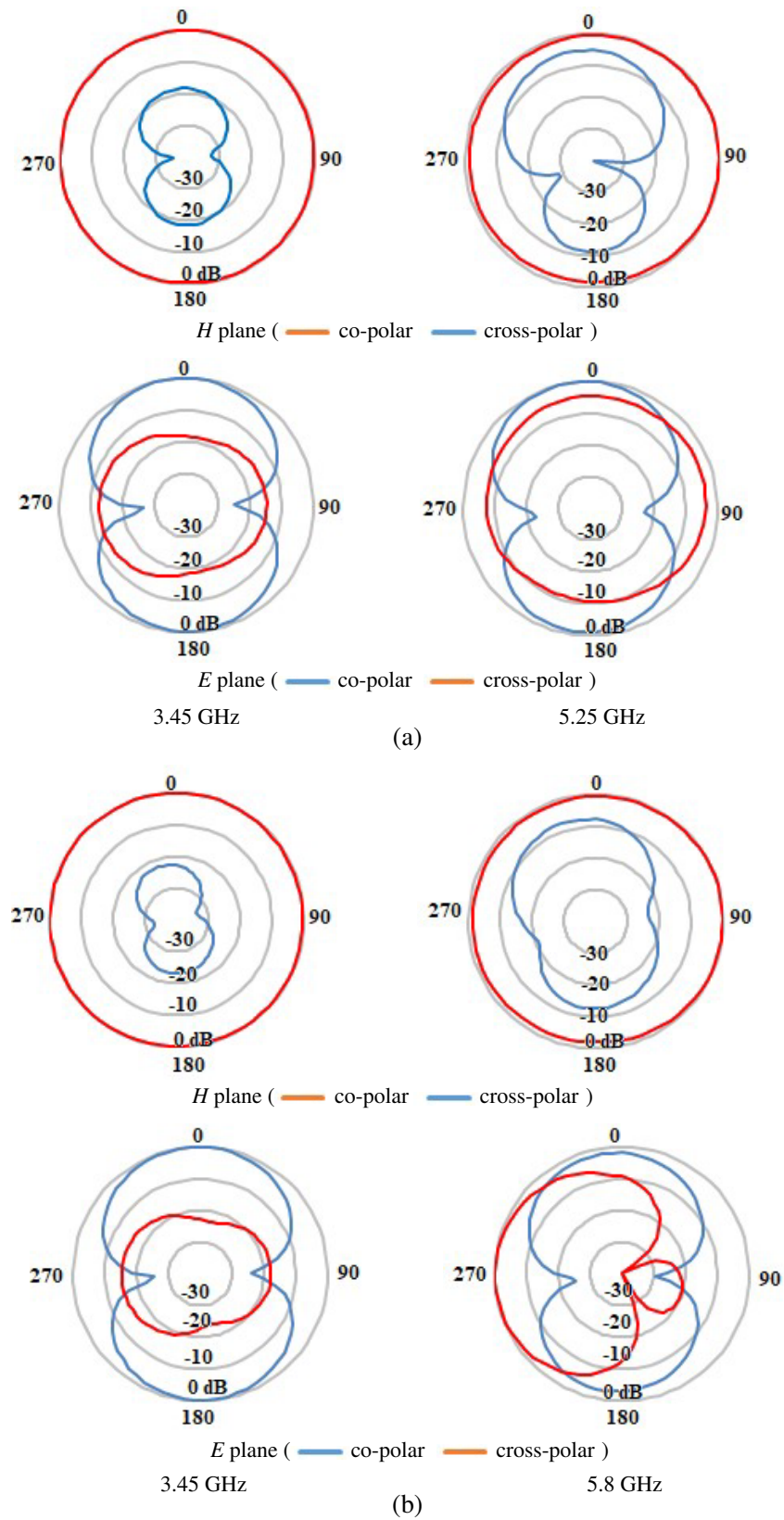
Figure 18. (a) Radiation patterns of proposed antenna PA1. (b) Radiation patterns of proposed antenna PA2.

S_{11} parameters are shown in Fig. 16, while measured and simulated gains of the antenna structures are shown in Fig. 17. The gain variation over the lower operating band is less than 1 dB, while the gain variation over the upper band is less than 2 dB. The measured results are in agreement with simulated ones. The measured radiation patterns in E-plane (X-Z plane) and H-plane (Y-Z plane) at 3.45 GHz and 5.25 GHz for PA1 and 3.45 GHz and 5.8 GHz for PA2 are shown in Fig. 18. The radiation patterns are nearly omnidirectional in the H-plane and figure of eight in the E plane. In PA1 and PA2, there is considerable surface current along x-axis (horizontal direction) which results in cross-polarization. At 3.45 GHz, the lower arm of right split ring becomes unresponsive and does not radiate as vector surface

Table 2. Comparison of proposed antenna with state of art reported multiband antennas.

Ref	Approach/Technique	Antenna Size (mm^2)	Bands (GHz)	% BW	Gain (dBi)	Electrical Size ($\lambda_o \times \lambda_o$)
[5]	Rectangular patch with pi and L-shaped slots for tri-band operation	27.5 × 20	2.37–2.52 3.35–3.9 4.95–7.85	6.13, 15.17, 45.31	3.9, 4.1, 3.8	$0.217 \times 0.158 = 0.0343\lambda_o^2$
[6]	Rectangular patch with inverted L-shaped slotted antenna with DGS for tri-band operation	20 × 30	2.39–2.51 3.15–3.91 4.91–6.08	4.898, 21.53, 21.29	1.9–6	$0.159 \times 0.239 = 0.038\lambda_o^2$
[14]	Elliptical ring with split triangular patch for dual-band operation	30 × 33	2.52–2.62 3.31–3.64	3.89 9.49	2.39, 1.75	$0.252 \times 0.277 = 0.070\lambda_o^2$
[15]	connected two rings on multilayer substrate for dual-band operation	60 × 40	0.88–1.03 1.47–2.74 3.32–5.97	15.71, 60.33, 57.05	−0.18, 3.66, 4.35	$0.176 \times 0.117 = 0.0206\lambda_o^2$
[17]	An elliptical shaped ring with parasitic patches for dual-band operation	180 × 60	0.66–0.79 3.28–3.78	17.93, 14.16	2.4, 6.1	$0.396 \times 0.132 = 0.0523\lambda_o^2$
[18]	Dual-Square Ring (DSR) excited through EM coupling of quadlateral ring for dual-band operation	24 × 24	2.34–2.48 3.68–3.89	5.08, 5.55	3.8, 4.3	$0.187 \times 0.187 = 0.035\lambda_o^2$
[19]	Nested dual square rings for tri-band operation	30 × 30	2.1–3.0 3.4–3.8 4.3–6.8	35.29, 11.11, 45.05	−2.0, −2.0, 2.0	$0.21 \times 0.21 = 0.0441\lambda_o^2$
[20]	ELC metamaterial based nested hexagonal ring for dual-band operation	30 × 30	2.77–4.12 4.45–5.42	39.19, 19.66	1.23, 1.57	$0.277 \times 0.277 = 0.0767\lambda_o^2$
[21]	CSRR engraved in rectangular patch for dual-band operation	34 × 20	1.78–1.90 3.45–6.58	6.52, 62.41	3.0, 3.16	$0.201 \times 0.118 = 0.0238\lambda_o^2$
[22]	Non-Bianisotropic CSRR engraved in rectangular patch for tri-band operation	29.4 × 26	2.5–3.61 4.06–4.59 4.8–6.07	36.33, 12.25, 23.36	Not Reported	$0.245 \times 0.217 = 0.0532\lambda_o^2$
PA1	Dual split ring connected through common branch for dual band operation	15 × 17	3.3–3.6 5.15–5.5	8.69, 6.75	1.1, 2.9	$0.165 \times 0.187 = 0.0308\lambda_o^2$
PA2	Dual split ring and a common closed ring branch for dual band operation	14 × 17	3.3–3.6 5.5–5.9	8.69, 7.02	1.0, 3.5	$0.154 \times 0.187 = 0.0283\lambda_o^2$

current density forms a loop, while at 5.25 GHz in PA1 and 5.8 GHz in PA2, this horizontal arm also radiates. This results in increase in cross polar component. In PA2, a slot is etched in top arm of PA1 to form a rectangular ring. There is significant surface current in this rectangular ring. At 3.45 GHz, the rectangular ring radiates in fundamental mode, while at 5.8 GHz it radiates in higher order mode. As a result, the radiation pattern degrades in E-plane. The cross-polar component also increases with frequency due to the increase in electrical thickness of the substrate and surface waves [25].

4. COMPARISON WITH STATE OF ART ANTENNAS

The proposed antennas (PA1 and PA2) are compared with state of art multiband antennas using slots or rings with respect to size and the techniques used in Table 2. The substrate dimensions of the proposed antenna structures are smaller than all the reported antennas except [15, 21]. The antenna in [15] is designed on multiple substrates (FR4 and glass) and therefore, difficult to fabricate as compared to the proposed antennas. The antenna in [21] is designed by engraving an SRR in a rectangular patch to operate over dual bands. However, it suffers from wide bandwidth in upper band due to coupling of modes generated by the patch and split ring. The proposed antenna does not suffer from this limitation. The two bands with the desired bandwidth can be easily obtained. All other antenna structures [5, 6, 14, 17–20, 22] have larger dimensions than the proposed antennas. The proposed structures have neither any complex SRR nor meta-material, and thus, the proposed antennas are simple to design.

5. CONCLUSION

Two compact dual-band antenna structures are proposed. In the first structure, a compact dual rectangular split ring monopole antenna is designed to operate over 3.3–3.6 GHz and 5.15–5.5 GHz for 5G and WLAN applications. The two split rings are connected through a common arm. In the second structure, a slot is cut in the upper arm of the first structure to form a closed rectangular ring. The antenna operates over 3.3–3.6 GHz and 5.5–5.9 GHz. The two bands can be easily controlled as the dimensions of two rings determine the resonant frequencies of the two bands. The antenna structures are simple to design. The antennas offer nearly omnidirectional radiation characteristics in both bands. The gain variation over the lower and upper bands is less than 1 dB and 2 dB, respectively. Thus, the proposed antenna structures are suitable for 5G and WLAN applications.

REFERENCES

1. Zaman, W., H. Ahmad, and H. A Mahmood, "Miniaturized meandered printed monopole antenna for triband applications," *Microwave and Optical Technology Letters*, Vol. 60, No. 5, 1265–1271, 2018.
2. Zhi, R., M. Han, J. Bai, W. Wu, and G. Liu, "Miniature multiband antenna for WLAN and X-band satellite," *Progress In Electromagnetics Research Letters*, Vol. 75, 13–18, 2018.
3. Cui, Y., L. Yang, B. Liu, and R. Li, "Multiband planar antenna for LTE/GSM/ UMTS and WLAN/WiMAX handsets," *IET Microwaves, Antennas & Propagation*, Vol. 10, No. 5, 502–506, 2016.
4. Osklang, P., C. Phongcharoenpanich, and P. Akkaraekthalin, "Triband compact printed antenna for 2.4/3.5/5 GHz WLAN/WiMAX applications," *International Journal of Antennas and Propagation*, Article ID 8094908, 2019.
5. Ahmad, H., W. Zaman, S. Bashir, and M. U. Rahman., "Compact triband slotted printed monopole antenna for WLAN and WiMAX applications," *Int. J. RF Microw. Comput. Aided Eng.*, Vol. 29, 2019.
6. Kunwar, A., A. K. Gautam, and B. K. Kanaujia, "Inverted L-slot triple-band antenna with defected ground structure for WLAN and WiMAX applications," *Int. J. Microwave and Wireless Technologies*, 1–6, 2015.

7. Jing, J., J. Pang, H. Lin, Z. Qiu, and C.-J. Liu, "A multiband compact low-profile planar antenna based on multiple resonant stubs," *Progress In Electromagnetics Research Letters*, Vol. 94, 1–7, 2020.

8. Ran, X., Z. Yu, T. Xie, Y. Li, X. Wang, and P. Huang, "A novel dual-band binary branch fractal bionic antenna for mobile terminals," *International Journal of Antennas and Propagation*, Article ID 6109093, 2020.

9. Wang, L., J. Yu, T. Xie, and K. Bi, "A novel multiband fractal antenna for wireless application," *International Journal of Antennas and Propagation*, Article ID 9926753, 2021.

10. Kaur, A. and P. K. Malik, "Multiband elliptical patch fractal and defected ground structures microstrip patch antenna for wireless applications," *Progress In Electromagnetics Research B*, Vol. 91, 157–173, 2021.

11. Asadallah, F. A., J. Costantine, and Y. Tawk, "A multiband compact reconfigurable PIFA based on nested slots," *IEEE Antennas and Wireless Propagation Letters*, Vol. 17, 331–334, 2018.

12. Bharadwaj, S. S., D. Sipal, D. Yadav, and S. K. Koul, "A compact tri-band frequency reconfigurable antenna for LTE/Wi-Fi/ITS applications," *Progress In Electromagnetics Research M*, Vol. 91, 59–67, 2020.

13. Singh, P. P., P. K. Goswami, S. K. Sharma, and G. Goswami, "Frequency reconfigurable multiband antenna for IoT applications in WLAN, Wi-MAX, and C-band," *Progress In Electromagnetics Research C*, Vol. 102, 149–162, 2020.

14. Dattatreya, G. and K. K. Naik, "A low volume flexible CPW-fed elliptical-ring with split-triangular patch dual-band antenna," *Int. J. RF Microw. Comput. Aided Eng.*, Vol. 29, 2019.

15. Yazdani, R., M. Yousefi, H. Aliakbarian, H. Oraizi, and G. A. E. Vandenbosch, "Miniaturized triple-band highly transparent antenna," *IEEE Transactions on Antennas and Propagation*, Vol. 68, No. 2, 712–718, 2020.

16. Fu, S., X. Zhao, C. Li, and Z. Wang, "Dual-band and omnidirectional miniaturized planar composite dipole antenna for WLAN applications," *Int. J. RF Microw. Comput. Aided Eng.*, Vol. 29, 2021.

17. Arya, A. K., S. J. Kim, and S. Kim, "A dual-band antenna for LTE-R and 5G lower frequency," *Progress In Electromagnetics Research Letters*, Vol. 88, 113–119, 2020.

18. Swain, B. R. and A. K. Sharma, "An investigation of dual-band dual-square ring (DSR) based microstrip antenna for WiFi/WLAN and 5G-NR wireless applications," *Progress In Electromagnetics Research M*, Vol. 86, 17–26, 2019.

19. Rosaline, S. I. and S. Raghavan, "Design of split ring antennas for WLAN and WiMAX applications," *Microwave and Optical Technology Letters*, Vol. 58, No. 9, 2117–2122, 2016.

20. Daniel, R. S., R. Pandeeswari, and S. Raghavan, "Dual-band monopole antenna loaded with ELC metamaterial resonator for WiMAX and WLAN applications," *Applied Physics A: Materials Science and Processing*, Vol. 124, No. 10, 1–7, 2018.

21. Prasad Jones Christydass, S. and N. Gunavathi, "Dual-band complementary split-ring resonator engraved rectangular monopole for GSM and WLAN/WiMAX/5G sub-6 GHz band," *Progress In Electromagnetics Research C*, Vol. 113, 251–263, 2021.

22. Pandeeswari, R., "A compact non-bianisotropic complementary split ring resonator inspired microstrip triple band antenna," *Progress In Electromagnetics Research C*, Vol. 81, 115–124, 2018.

23. Kumar, G. and K. P. Ray, *Broadband Microstrip Antennas*, Artech House, Norwood, MA, 2003.

24. Ray, K. P., "Design aspects of printed monopole antennas for ultra-wide band applications," *International Journal of Antennas and Propagation*, Vol. 2008, 1–8, 2008.

25. Mishra, S. K., R. K. Gupta, and J. Mukherjee, "Effect of substrate material on radiation characteristics of an UWB antenna," *Loughborough Antennas & Propagation Conference*, 157–160, U.K., 2010.